JOURNAL OF CATALYSIS **160,** 155–170 (1996)
ARTICLE NO. 0135

# Yttria-Stabilized Zirconia Supported Copper Oxide Catalyst

## I. Effect of Oxygen Vacancy of Support on Copper Oxide Reduction

Wei-Ping Dow, Yu-Piao Wang, and Ta-Jen Huang[1]

*Department of Chemical Engineering, National Tsing Hua University, Hsinchu, Taiwan 300, Republic of China*

Received September 27, 1994; revised October 20, 1995; accepted January 23, 1996

**Copper oxide was supported on yttria-stabilized zirconia (YSZ) and $\gamma$-alumina, respectively, using impregnation methods. The reducibility and characteristics of the supported copper oxide catalysts with various copper loadings were revealed and determined by temperature-programmed reduction (TPR) and electron paramagnetic resonance (EPR), respectively. For CuO/$\gamma$–alumina catalyst, only two peaks were found in the TPR patterns. One with lower peak temperature has been attributed to the reduction of highly dispersed copper ions; the other with higher peak temperature has been ascribed to the reduction of bulk-like copper oxide. For CuO/YSZ catalyst, four TPR peaks could be observed. Two TPR peaks with lower peak temperatures (namely, $\alpha_1$ and $\alpha_2$) have been attributed to the hydrogen uptake of nested oxygen ions (NOIs) and temptable oxygen ions (TOIs), respectively. These are interface-boundary terminal oxygen ions of the supported copper oxide but have different environment and interaction with the surface oxygen vacancies of the YSZ support. The other two TPR peaks of CuO/YSZ catalyst were formed with the same reason as occurring on the CuO/$\gamma$–alumina. EPR has confirmed these structures and environments of these supported copper oxides. Two reduction mechanisms have been proposed for hydrogen reacting with the NOIs and the TOIs, respectively. The former case has been attributed to the function of oxygen-ionic transport of the YSZ support. The latter case was owing to the oxygen vacancies of YSZ acting as Lewis acid sites. In addition, a small but sharp TPR peak occurring at ca. 657°C was found in the TPR pattern of YSZ support. This peak has been attributed to the hydrogen uptake of surface capping oxygen ions of YSZ support which are coordinated beside the surface oxygen vacancies of YSZ.** 

### 1. INTRODUCTION

Carbon monoxide oxidation is an important reaction for the treatment of automobile exhaust. Copper oxide has been demonstrated to be a very active species among the base-metal oxides for this reaction (1, 2). Hence, many studies have been focused on copper-based catalysts (3–6). However, when copper oxide is supported on traditional support (e.g., alumina), it still seems that one cannot obtain a catalytic activity which can compete with precious metals. On the other hand, the selectivity and activity of CO hydrogenation has been improved by the metal–support interaction (7, 8). Hence, if one would like to enhance the catalytic activity of supported copper oxide, it seems to be a feasible way that chooses a proper support to make some kind of metal–support interaction or synergistic effect.

It has been shown that the supports such as $Y_2O_3$-stabilized $ZrO_2$ (YSZ) (9, 10) and $Gd_2O_3$-doped $CeO_2$ (11), which possess oxygen vacancies and oxygen-ionic conductivity, can enhance the activities of Pt and Rh catalysts for CO oxidation and NO reduction, respectively. These have been attributed to the oxygen storage/transport characteristics in the support and to the generation of very active centers existing at the interface between metal and support. In our previous study (12), this effect is also found on copper oxide catalyst supported on the YSZ.

Many studies have demonstrated that the oxygen vacancies of metal oxides such as vanadium oxide (13), copper oxide (14), and superconducting oxides (15) can enhance the activities of these catalysts for CO oxidation. Moreover, Ekerdt and co-workers (16–18) recently confirmed that the active sites for CO hydrogenation over YSZ and CaO-stabilized $ZrO_2$ (CSZ) are oxygen vacancies and they also found that the higher mobility of oxygen vacancy is, the higher reaction rate becomes.

Klissurski and Rives (15) pointed out that the lower binding energy for oxygen in base-metal oxide is, the lower onset temperature of this oxide during TPR is observed and leads to a higher catalytic activity in CO oxidation. Hence, when copper oxide is supported on YSZ the metal–support interfacial reaction step which includes adsorbed oxygen instead of lattice oxygen can significantly enhance the catalytic activity of CuO/YSZ catalyst for CO oxidation (12). For hydrocarbon oxidation, a similar relationship between catalytic oxidation activity of metal oxide catalysts and its bond strength of terminal oxygen has also been reported by Andersson *et al.* (19).

[1] To whom correspondence should be addressed.



0021-9517/96 $18.00

For comparison with CuO/YSZ and interpreting the TPR and EPR results of CuO/YSZ, the TPR and EPR of CuO/$\gamma$-$Al_2O_3$ were also carried out in this work. In fact, $\gamma$-alumina supported copper oxide catalysts have been studied by many authors (3, 20–26). The structure of copper oxide and the environment of copper ions supported on alumina is complicated. However, only two types of copper ions, isolated (well-dispersed) and clustered (bulk-like) ions, are usually and easily detectable by using X-ray photoelectron spectroscopy (XPS) (20, 22), TPR (23), EPR (26–28), and X-ray diffraction (XRD) (3, 20, 22), although Tikhov and co-workers (24, 25) could distinguish various types of copper oxide species existing on alumina support. Nevertheless, a quantitative study between these two types of copper ions and their reducibility and reoxidability is still wanting. TPR is a good method of qualitatively and quantitatively characterizing the reducible catalyst without an ultrahigh vacuum (UHV) system.

In practice, stabilized zirconia has been the subject of great interest because of its practical applications as a solid electrolyte for oxygen sensors and fuel cells (29, 30). On the contrary, there are only a few studies so far that use the stabilized zirconia as a support. It has been reported that zirconia has three well-defined polymorphs, namely, monoclinic, tetragonal, and cubic (31). The pure zirconia, normally in monoclinic phase at room temperature, may be stabilized in cubic phase by the addition of variable amounts of $R_2O_3$ (R, rare earth or yttrium) or CaO (29–32). Oxygen vacancies can be created in the cubic crystalline structure of YSZ by introducing substitutional trivalent ions $Y^{3+}$ (30–32). These vacancies increase the electrical conductivity with diffusing oxygen ions being the primary charge carrier. The transport properties of YSZ depend on the oxygen vacancy concentration and the ionic conductivity reaches a maximum at about 8–10 mol% $Y_2O_3$ and then decreases rapidly (30, 31).

Therefore, this work will employ the TPR and EPR to investigate the environment and structure of the YSZ supported copper oxide. In addition, this work will study the effect of oxygen vacancies of YSZ support on the reduction behaviors of supported copper oxide catalysts to confirm the existence of interfacial active center due to the oxygen vacancies of YSZ. The effect of oxygen vacancies of YSZ support on the catalytic activity of supported copper oxide catalysts for CO oxidation will be presented in Part II of this work (33). Results indicate that the interfacial copper oxides are accessible to the oxygen vacancies of YSZ support and reduced at very low temperatures.

## 2. EXPERIMENTAL

*Catalyst preparation and characterization.* The catalysts were prepared by impregnating 8 mol% YSZ (Dowa Chemical, Japan, 0.35 $\mu$m, yttria content is 8 mol%.) and $\gamma$-alumina (Strem, USA, 150–200 mesh) with an appropriate amount of aqueous solution of copper nitrate (Strem, 99.999%). After evaporating the excess water at ca. 80°C, the catalysts were dried in air at 120°C for 24 h and then calcined in air at 260°C for 1.5 h and subsequently at 500°C for 3.5 h. Those as-calcined catalysts will be called fresh catalysts in latter results and discussion. The BET areas of the catalysts were determined by means of nitrogen physisorption, applying a thermal conductivity detector (TCD) instrument.

*Temperature-programmed reduction (TPR).* TPR of catalyst was carried out using 10% hydrogen in nitrogen as reducing gas. Gas flow rate was 30 ml/min and adjusted by mass flow controllers. The gas flow system of the TPR apparatus was composed of two six-pore valves. Hydrogen consumption of the TPR was detected by a TCD and its signal was transmitted to a personal computer. The peak areas of TPR could also be separated and integrated by this computer using a special software. The temperature of the catalyst sample was controlled by a temperature-programmable controller (Eurotherm, Model 815P). The cell used for TPR was made of 8-mm-i.d. quartz U-tube and the catalyst sample of 100 or 200 mg was mounted on loosely packed quartz wool. The outlet of TPR cell was connected to a glass column packed with molecular sieve 5A in order to remove the moisture produced from reduction.

For comparison with the TPR result of YSZ support, TPR of pure zirconia (Johnson Matthey, 325 mesh, 99.7%) and yttria (Johnson Matthey, 325 mesh, 99.99%) was also carried out. The sample weight was 200 mg and the heating rate of TPR was 20°C/min. The other experimental steps are the same as mentioned above.

*Reoxidation treatment.* The purpose of the reoxidation treatment is to separate shoulder peak in TPR patterns. The latent peak of TPR patterns can also be revealed its deserved feature by reoxidation, which causes the supported copper oxide to be redispersed (see Results and Discussion).

Before reoxidation, the catalyst was conducted with a TPR. The TPR method has been described as above. The reduction temperature was raised from room temperature to 500°C and then held at 500°C for 1 h. Subsequently, the catalyst temperature was decreased to a desired one (i.e., 100, 300, or 500°C) and the gas flow was simultaneously switched to air with a flow rate of 30 ml/min. The time of reoxidation was 1 h. After each TPR run of the reoxidized catalyst which had been treated at certain reoxidation temperature, the sample packed in the cell would be renewed and a fresh catalyst would be replenished into the cell. In other words, whichever reoxidation temperature was chosen, the initial state of the reoxidized catalyst was the fresh catalyst.

*Electron paramagnetic resonance (EPR) measurement.* It is well-known that EPR can characterize the structure

and environment of copper oxide and judge the dispersed extent of supported copper oxide. The EPR measurements were carried out with a Bruker ER 200D spectrometer operating in X-band (ca. 9.7 GHz). The magnetic field was modulated at 100 kHz. The $g$ values were obtained by comparison with a diphenylpicrylhydrazyl (DPPH) standard ($g = 2.0036$). Before each EPR measurement, the catalyst was dried in air at 120°C for 24 h. All the EPR measurements were performed at room temperature.

## 3. RESULTS

The characteristics of various fresh catalysts are summarized in Table 1. The decrease in BET area of $\gamma$-$Al_2O_3$ after calcination is presumably caused by the plugging of some micropores due to the loading of copper oxide (12), whereas the BET area of YSZ support does not vary with increasing the copper loading. Since YSZ is a crystalline oxide (30, 31), it has less rough surface and possesses few pores. Hence, the BET area is mainly contributed from the external surface.

The colors of the CuO/$\gamma$-$Al_2O_3$ catalysts coincide with those of literature (3, 34) and it was confirmed that when the dark or black color is observed, the bulk copper oxide is formed. This agrees with the TPR results in this study (see below). The colors of the CuO/YSZ catalysts are different from those of CuO/$\gamma$-$Al_2O_3$ catalysts. Black color is not observed on CuO/YSZ, however, the higher the copper loading is, the darker the color will be observed.

### 3.1. TPR of CuO/$\gamma$-$Al_2O_3$ Catalyst

Two peaks, $\beta$ and $\gamma$, could be distinguished on the TPR curves, as shown in Fig. 1. The area of $\gamma$ peak obviously increases with increasing the copper loading, but the area of $\beta$ peak has a maximum value occurring at 7.5 wt% Cu.

**TABLE 1**

**Characteristics of Fresh Catalysts**

| Support | Copper loading (wt%) | BET area ($m^2/g$) | Color |
|---|---|---|---|
| $\gamma$-$Al_2O_3$ | 0.0 | 169.5 | White |
| | 2.5 | 139.3 | Clear blue |
| | 5.0 | — | Green-blue |
| | 7.5 | — | Olive-green |
| | 10.0 | 120.2 | Dark green |
| | 12.5 | — | Dark gray |
| | 15.0 | 109.9 | Black |
| | 30.0 | — | Black |
| YSZ | 0.0 | 10.1 | White |
| | 0.2 | 10.1 | Light-white blue |
| | 0.4 | 10.4 | Light gray |
| | 0.6 | 10.3 | Light-ashen yellow |
| | 0.8 | 10.3 | Ashen yellow |
| | 1.0 | 10.3 | Ashen yellow |
| | 1.5 | 10.2 | Gray |

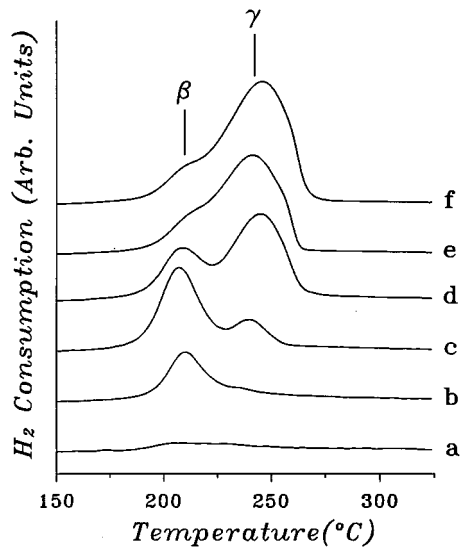


**FIG. 1.** TPR patterns of CuO/$\gamma$-$Al_2O_3$ catalysts. Operating conditions: 10°C/min, 10% $H_2$ in $N_2$, with total flow rate of 30 ml/min. Sample weight, 100 mg. Catalysts: (a) 2.5 wt% Cu, (b) 5.0 wt% Cu, (c) 7.5 wt% Cu, (d) 10.0 wt% Cu, (e) 12.5 wt% Cu, (f) 15.0 wt% Cu.

When the copper loading is lower than 7.5 wt%, the $\gamma$-peak area is smaller than that of $\beta$-peak, and when the copper loading is higher than 7.5 wt% the $\gamma$-peak area is larger than that of $\beta$-peak and the $\beta$ peak becomes a shoulder. In addition, overlap of $\beta$ and $\gamma$ peaks becomes very serious when copper loading is larger than 12.5 wt%. This implies that the amount of $\beta$-peak copper oxide species is limited by a certain factor. In other words, it seems to have a saturated phenomenon occurring at 7.5 wt% Cu for $\beta$ peak. The serious overlap of $\beta$ and $\gamma$ peaks implies that the chemical reactivity (i.e., reducibility) of these two types of copper oxide species gradually approaches to the same.

For quantitative analysis, all of the peaks that can be discerned by computer software have been integrated to evaluate their individual amounts. The numerical values are given in Table 2. The fraction of peak area represented in terms of percentage is defined as one peak area divided by total peak area in this sample. Evidently, there is a maximum fraction of $\beta$-peak area existing at 7.5 wt% Cu for fresh catalyst. Considering the absolute amount of hydrogen consumption of these catalysts, the order of magnitude of $\beta$-peak area is the same as that of their relative percentages.

### 3.2. TPR of Reoxidized Cu/$\gamma$-$Al_2O_3$ Catalyst

In order to confirm that there was a saturated phenomenon for certain copper ions (i.e., $\beta$-peak species), reoxidations of 10 and 12.5 wt% Cu/$\gamma$-$Al_2O_3$ catalysts were carried out. The TPR patterns of these reoxidized catalysts are shown in Figs. 2 and 3, respectively. The extent of reoxidation is referred to the $H_2$/Cu ratio of TPR.

**TABLE 2**

**The Integrated Values of TPR Peaks of CuO/$\gamma$-$Al_2O_3$ Catalysts[a]**

| | Fresh catalyst | | | | Reoxidized catalyst[b] | | | |
|---|---|---|---|---|---|---|---|---|
| | Absolute amount | | Relative value | | Absolute amount | | Relative value | |
| Copper Loading (wt%) | $\beta$ Peak (mol $H_2$) $\times 10^{-5}$ | $\gamma$ Peak (mol $H_2$) $\times 10^{-5}$ | $\beta$ Peak (%) | $\gamma$ Peak (%) | $\beta$ Peak (mol $H_2$) $\times 10^{-4}$ | $\gamma$ Peak (mol $H_2$) $\times 10^{-5}$ | $\beta$ Peak (%) | $\gamma$ Peak (%) |
| 5.0 | 4.80 | 3.07 | 61 | 39 | — | — | — | — |
| 7.5 | 7.91 | 3.90 | 67 | 33 | — | — | — | — |
| 10.0 | 5.04 | 10.70 | 32 | 68 | 1.29 | 2.8 | 82 | 18 |
| 12.5 | 4.92 | 14.80 | 25 | 75 | 1.12 | 8.5 | 57 | 43 |
| 15.0 | 4.25 | 19.40 | 18 | 82 | — | — | — | — |
| 30.0 | 3.78 | 43.50 | 8 | 92 | — | — | — | — |

[a] Operating conditions of TPR: reducing gas, 10% $H_2/N_2$; flow rate, 30 ml/min; heating rate, 10°C/min; sample weight, 100 mg.
[b] Reoxidized in air at 500°C for 1 h.

For 10 wt% Cu catalyst, the extent of reoxidation at 300 and 500°C is approximately the same but the $\gamma$ peak almost disappears and the $\beta$ peak becomes larger than that of the fresh one. For 12.5 wt% Cu catalyst, the $\beta$ peak also becomes larger after reoxidation at 300 and 500°C as compared with that of the fresh one, but the $\gamma$ peak still exists. In addition, the reoxidized extent at 300°C reduces to the $H_2$/Cu ratio of 0.88. This indicates that the lower the copper loading is, the higher the reoxidability of copper catalyst that can be observed. However, both 10 and 12.5 wt% Cu catalysts have lower reoxidized extent under a reoxidation temperature of 100°C. Again, the reoxidized extent of the 12.5 wt% Cu catalyst is still lower than that of the 10 wt% one.

These reoxidized extents and TPR behaviors of these reoxidized catalysts indicate that when the copper loading is lower than 10 wt%, the $\gamma$-peak copper species can be almost completely transformed into the $\beta$-peak one following the reoxidation of which the treated temperature is higher than 300°C. When the copper loading is higher than 10 wt%, the $\gamma$-peak copper species cannot be completely transformed into the $\beta$-peak one. This seems to imply that this transformation between the $\beta$ and the $\gamma$ peak is limited. The numerical values of the TPR peak areas of the reoxidized catalysts are also evaluated and listed in Table 2. Indeed, there is a marked change in the percentage of peak area when the catalysts have undergone the reoxidation treatment.

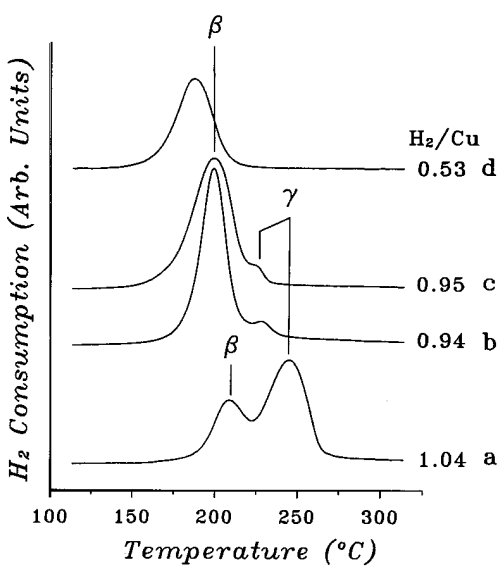


**FIG. 2.** TPR patterns of reoxidized 10.0 wt% Cu/$\gamma$-$Al_2O_3$ catalyst. Operating conditions are as in Fig. 1. Sample weight, 100 mg. (a) Fresh catalyst, (b) reoxidized at 500°C, (c) reoxidized at 300°C, (d) reoxidized at 100°C. The initial state of (b), (c), and (d) is fresh catalyst.

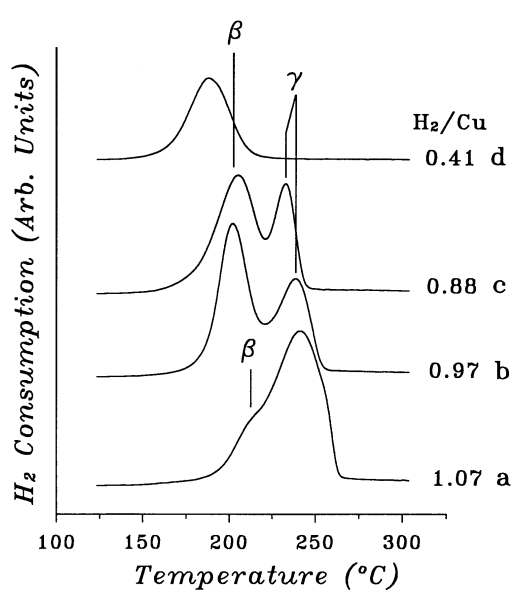


**FIG. 3.** TPR patterns of reoxidized 12.5 wt% Cu/$\gamma$-$Al_2O_3$ catalyst. Operating conditions are as in Fig. 1. Sample weight, 100 mg. (a), (b), (c), and (d), as in Fig. 2.

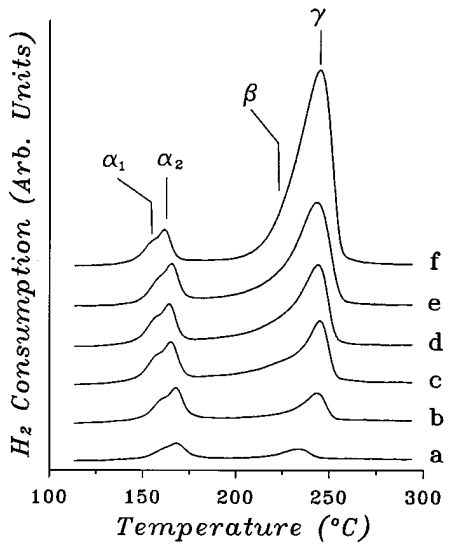


**FIG. 4.** TPR patterns of CuO/YSZ catalysts. Operating conditions are as in Fig. 1. Sample weight, 200 mg. Catalysts: (a) 0.2 wt% Cu, (b) 0.4 wt% Cu, (c) 0.6 wt% Cu, (d) 0.8 wt% Cu, (e) 1.0 wt% Cu, (f) 1.5 wt% Cu.

It is remarkable that the serious overlap of the $\beta$ and the $\gamma$ peak for 12.5 wt% Cu/$\gamma$-$Al_2O_3$ catalyst has been distinctly separated by the reoxidation treatment at 300°C. This result suggests that if there is a shoulder or latent peak in the TPR pattern, its deserved feature can be revealed by the reoxidation treatment due to its different reoxidability. This experimental skill will also be employed for the characterization of Cu/YSZ catalysts.

### *3.3. TPR of CuO/YSZ Catalyst*

It is very interesting that when copper oxide is supported on YSZ, there is a third peak, $\alpha$, to be observed in its TPR pattern as well as $\beta$ and $\gamma$ peaks. The $\alpha$ peak consists of $\alpha_1$ and $\alpha_2$ peaks, in which $\alpha_1$ is a shoulder of $\alpha_2$. Additionally, the $\beta$ peak of CuO/YSZ catalyst becomes a latent one. All the TPR patterns of the CuO/YSZ catalysts are shown in Fig. 4.

It is worth noting that the $\alpha$-peak temperature is very low compared with that of the $\beta$ or $\gamma$ peak as shown in Fig. 4 and with that of the $\beta$ or $\gamma$ peak of CuO/$\gamma$-$Al_2O_3$ as shown in Fig. 1. Hence, the reduction of $\alpha$-peak species seems to be an extrinsic behavior of copper oxide. It is believed that a certain induction factor, which can enhance the reducibility of the supported copper oxide to create the $\alpha$ peak, must exist on the CuO/YSZ catalyst. Moreover, this induction factor should come from the YSZ support.

When copper oxide was supported on zirconia, two peaks were also found in TPR patterns (35). However, the peak temperatures of these two TPR peaks are very close to those of $\beta$ and $\gamma$ peaks of CuO/YSZ catalyst in this work. Shimokawabe *et al.* (35) attributed these two TPR peaks of CuO/$ZrO_2$ to the reductions of highly dispersed CuO and/or $Cu^{2+}$ ions in an octahedral environment and bulky CuO, respectively.

According to the integrated results of TPR peaks listed in Table 3 and considering the relative values of peak areas, the maximum percentage occurs at 0.4 wt% Cu for the $\alpha_1$ peak, 0.2 wt% Cu for the $\alpha$ peak, and 1.5 wt% Cu for the $\beta+\gamma$ peak, respectively. The amounts of $\beta$- and $\gamma$-peak copper oxide species monotonously increase with increasing copper loading but the $\alpha_1$- and the $\alpha_2$-peak copper oxide species do not. Considering the absolute amount of hydrogen consumption, the maximum value occurs at 0.4 wt% Cu for the $\alpha_1$ peak, 0.6 wt% Cu for the $\alpha$ peak, and 1.5 wt% Cu for the $\beta+\gamma$ peak. These results are different from that of the CuO/$\gamma$-$Al_2O_3$, of which the order of magnitude of relative peak fraction coincides with that of absolute amounts. Hence, the amount of $\alpha$-peak copper oxide species is not only limited by the BET area of the YSZ support but also related to its environment, which includes an induction factor originating from the YSZ support.

**TABLE 3**

**The Integrated Values of TPR Peaks of CuO/YSZ Catalysts[a]**

| | Fresh catalyst | | | | | | Reoxidized catalyst[b] relative value | |
|---|---|---|---|---|---|---|---|---|
| | Absolute amount | | | Relative value | | | | |
| Copper Loading (wt%) | $\alpha_1$ Peak (mol $H_2$) $\times 10^{-7}$ | $\alpha$ Peak[c] (mol $H_2$) $\times 10^{-7}$ | $\beta+\gamma$ Peak (mol $H_2$) $\times 10^{-6}$ | $\alpha_1$ Peak (%) | $\alpha$ Peak[c] (%) | $\beta+\gamma$ Peak (%) | $\alpha$ Peak[c] (%) | $\beta+\gamma$ Peak (%) |
| 0.2 | 6.11 | 36.41 | 2.66 | 9.7 | 57.8 | 42.2 | — | — |
| 0.4 | 30.36 | 61.35 | 6.46 | 24.1 | 48.7 | 51.3 | — | — |
| 0.6 | 25.89 | 69.54 | 11.94 | 13.7 | 36.8 | 63.2 | 30 | 70 |
| 0.8 | 20.91 | 63.75 | 18.82 | 8.3 | 25.3 | 74.7 | — | — |
| 1.0 | 20.16 | 62.68 | 25.23 | 6.4 | 19.9 | 80.1 | — | — |
| 1.5 | 15.59 | 53.86 | 41.86 | 3.3 | 11.4 | 88.6 | — | — |

[a] Operating conditions of TPR: same as in Table 2.
[b] Reoxidized in air at 500°C for 1 h.
[c] $\alpha$ Peak area = $\alpha_1$ peak area + $\alpha_2$ peak area.

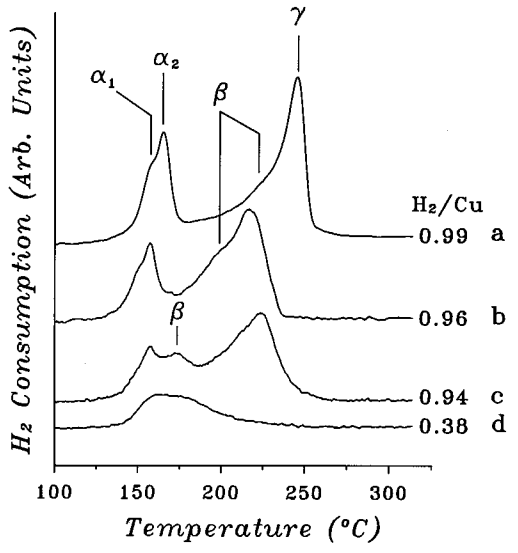


**FIG. 5.** TPR patterns of reoxidized 0.6 wt% Cu/YSZ catalyst. Operating conditions are as in Fig. 1. Sample weight, 200 mg. (a), (b), (c), and (d), as in Fig. 2.

### *3.4. TPR of Reoxidized Cu/YSZ Catalyst*

It has been mentioned in Section 3.2 that if there is a latent peak existing in TPR pattern, it can be revealed by means of reoxidation treatment. Indeed, the $\beta$ peaks of the 0.6 and 1.0 wt% Cu/YSZ catalysts became distinguishable after reoxidation at 300 °C. These results are shown in Figs. 5 and 6, respectively.

It is evident that the original $\beta$ peak of the 0.6 wt% Cu/YSZ catalyst is a latent peak as shown in Fig. 5a; subsequently, it becomes a shoulder after it has undergone a reoxidation treatment at 500°C, as shown in Fig. 5b. When it is reoxidized at 300°C, the $\beta$ peak becomes a discernible one, as shown in Fig. 5c. Similar result is also found in the case of 1.0 wt% Cu/YSZ catalyst as shown in Fig. 6.

A noteworthy result is that the relative percentage and reduction temperature of $\alpha$ peak is almost not altered by the reoxidation treatment. The percentages of the reoxidized peak areas are given in Table 3. In addition, the profiles of $\alpha_1$ and $\alpha_2$ peaks shown in Figs. 5b and 6b were also not modified by the reoxidation treatment. Therefore, the reoxidized results seem to reveal that the $\alpha$-peak formation is not due to the reduction of highly dispersed copper ions (i.e., isolated $Cu^{2+}$ ions) but due to certain induction factor derived from the YSZ support, because its relative percentage is almost not affected by the reoxidation treatment. This will be confirmed by the following EPR results. On the other hand, the $\beta$- and the $\gamma$-peak temperatures of the reoxidized CuO/YSZ catalysts were shifted toward the lower one after the reoxidation treatment. This shift behavior of TPR peak is similar to that of the reoxidized Cu/$\gamma$-$Al_2O_3$ catalyst. Hence, the reduction of $\beta$- and $\gamma$-peak copper oxide species of Cu/YSZ catalyst is believed to be an intrinsic behavior, which does not include any induction factor.

When the 0.6 wt% Cu/YSZ was reoxidized at 100°C, a small and broadened peak was observed as shown in Fig. 5d. This can be attributed to the reduction of surface layer and/or sublayer copper oxide, which has also been found in the case of Cu/$\gamma$-$Al_2O_3$.

### *3.5. TPR of YSZ Support*

Figure 7 shows the TPR patterns of high-temperature range. A small but sharp peak, $\delta$ as shown in Fig. 7c, is observed with a peak temperature of 657°C. This $\delta$ peak of YSZ support would be broadened and shifted toward a lower temperature due to the existence of copper.

It is found that the end temperature of the $\delta$ peak seems to be not affected by the existence of copper, whereas both initial and peak temperatures are accessible to the existence of copper. In order to confirm this, peak integration was calculated by computer with a same end temperature but with different initial temperatures of these $\delta$ peaks. Indeed, as shown in Fig. 8, when the temperature range of integration is chosen from 385 to 725°C, the total hydrogen consumption is approximately independent of the copper loading. On the other hand, the hydrogen consumption of the $\delta$ peak is reduced with increasing the copper loading when the temperature range of integration is chosen from 525 to 725°C. This suggests that the more metal copper species exist on the surface of YSZ, the more easily YSZ support can be reduced by hydrogen.

For the sake of understanding the derivation of the $\delta$ peak, the TPR of pure yttria and zirconia were also carried out and shown in Figs. 7a and 7b, respectively. Obviously,

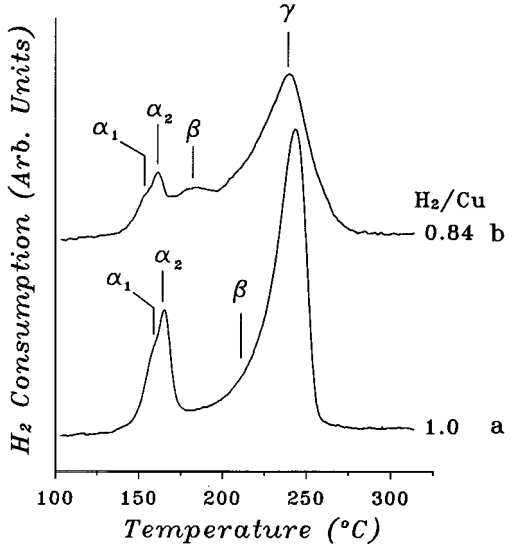


**FIG. 6.** TPR patterns of reoxidized 1.0 wt% Cu/YSZ catalyst. Operating conditions are as in Fig. 1. Sample weight, 200 mg. (a) Fresh catalyst, (b) reoxidized at 300°C. The initial state of (b) is fresh catalyst.

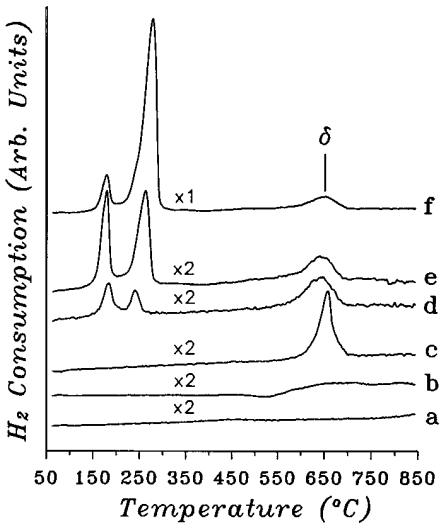


**FIG. 7.** TPR patterns in high temperature range. Operating conditions: 20°C/min; the rest are as in Fig. 1. Sample weight, 200 mg. (a)$Y_2O_3$, (b) $ZrO_2$, (c) 8 mol% YSZ support, (d) 0.2 wt% Cu/YSZ catalyst, (e) 0.6 wt% Cu/YSZ catalyst, (f) 1.5 wt% Cu/YSZ catalyst. ( $\times 1$, $\times 2$) Relative scale.

yttria is not easily reduced by hydrogen until 850°C. The initial TPR temperature of zirconia is lower than that of the $\delta$ peak of YSZ support. The TPR peak of zirconia is very small and broadened, and its TPR curve seems to not return to the baseline even after 800°C. This reduction behavior of zirconia is entirely different from that of YSZ. Based on the results of literature (35–38), the broadened TPR peak of zirconia can be ascribed to the reduction of $Zr^{4+}$ to $Zr^{3+}$, which occurs only at the surface layer and/or in the sublayer of zirconia. Thus, the $\delta$-peak formation becomes especially interesting.

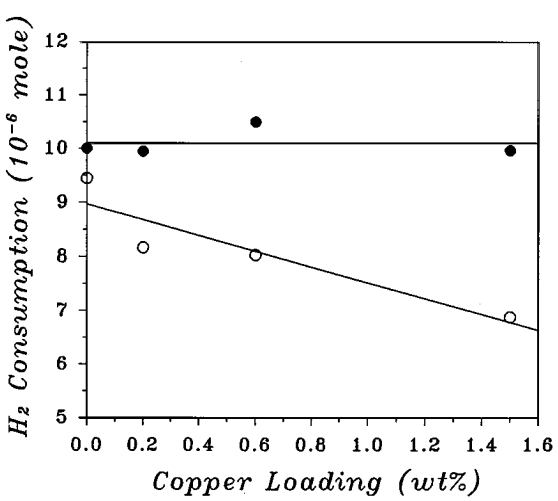


**FIG. 8.** Relationship between hydrogen consumption of $\delta$ peak and copper loading. (●) Integrated temperature range of $\delta$ peak, 385 to 725°C; (○) integrated temperature range of $\delta$ peak, 525 to 725°C.

### 3.6. EPR

*CuO/$\gamma$-alumina catalyst.* Figure 9 shows the typical EPR spectra of the CuO/$\gamma$-alumina catalysts investigated. These EPR spectral parameters (i.e., $g_\perp$=2.041; $g_\parallel$ = 2.33; $A_\parallel$=145G) has been interpreted as arising from the distorted octahedrally coordinated $Cu^{2+}$ ions (25, 39). The four-line hyperfine splittings indicate that there are isolated $Cu^{2+}$ ions ($I = 3/2$) on the $\gamma$-alumina surface (27, 39–41).

When the copper contents are increased, a poorly resolved hyperfine structure is observed and the signal intensities of the EPR spectra also significantly decrease. These are due to dipolar coupling arising from the strong interaction of near-neighbor copper atoms and the cluster formation experiencing antiferromagnetic couplings, which make them undetectable by EPR (28, 39–41). These also imply that a great part of these isolated $Cu^{2+}$ ions are buried in multilayered crystallites whose spatial structure approaches that of a normal CuO lattice. Nevertheless, the hyperfine structure can still be observed in the EPR spectrum of 15 wt% Cu/$\gamma$-alumina catalyst. Similar results were also found by Blanco *et al.* (40) over $CuCl_2$/$\gamma$-alumina catalysts.

*CuO/YSZ catalyst.* Essentially, as shown in Fig. 10, the EPR spectra of CuO/YSZ catalysts are similar to those of

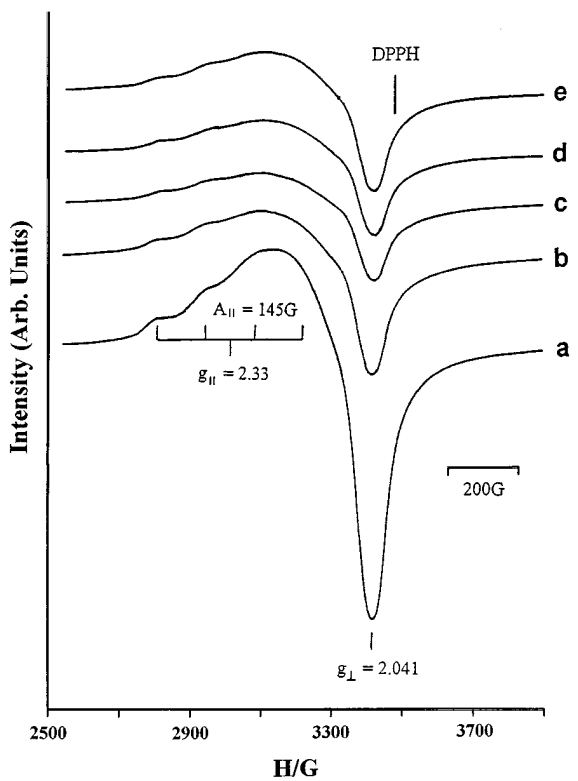


**FIG. 9.** EPR spectra of CuO/$\gamma$-alumina catalysts recorded at room temperature. Copper loadings: (a) 2.5 wt%, (b) 5 wt%, (c) 7.5 wt%, (d) 10 wt%, (e) 15 wt%.

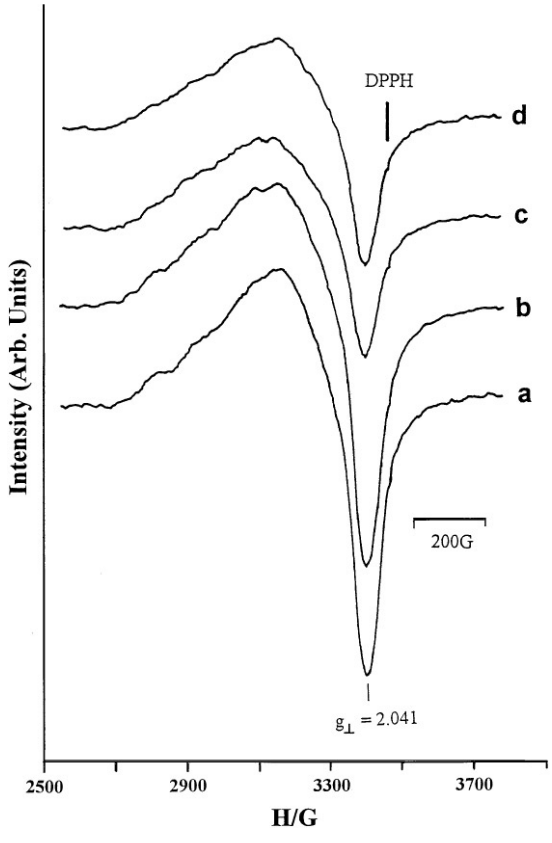


**FIG. 10.** EPR spectra of CuO/YSZ catalysts recorded at room temperature. Copper loadings: (a) 0.2 wt%, (b) 0.4 wt%, (c) 0.6 wt%, (d) 1.5 wt%.

CuO/$\gamma$-alumina catalysts. However, the hyperfine splitting is so weak that it is difficult to obtain their $g_\parallel$ value and $A_\parallel$ constant. When the copper loading increases up to 1.5 wt%, the hyperfine structure almost disappears. These imply that most of the copper species supported on the YSZ support are not the isolated $Cu^{2+}$ ions, but, especially of the higher copper loading one, the weak magnetic copper–oxygen associates. This EPR result is a key point for explaining the reason of $\alpha$-peak formation. This will be interpreted under Discussion.

It has been reported that when copper oxide is supported on $CeO_2$, which is also an oxygen-ion conducting material and also possesses the cubic fluorite-type structure (30, 42–44), and calcined at temperature above 400°C, a signal K defined in previous works (41, 45) can be observed in the EPR spectrum. This signal K had been attributed to a pair of two equivalent $Cu^{2+}$ ions separated by a distance of 3.4 Å and coordinated with a oxygen ion that locates between them at the $CeO_2$ surface, which can be easily reduced by $H_2$ or $C_2H_4$ (45). However, we did not find this signal in the EPR spectra of CuO/YSZ catalysts. Hence, the $\alpha_1$-peak copper oxide species cannot be judged to be the copper ions that can create the signal K in EPR.

## 4. DISCUSSION

### *4.1 Reduction and Reoxidation Behaviors of CuO/$\gamma$-$Al_2O_3$ Catalyst*

In fact, the structure and coordination environment of the $\gamma$-alumina supported copper oxide have been thoroughly studied by many authors using many physical methods (20, 22, 25, 27, 28, 39). According to the literature (20, 22, 25, 27, 28, 39), the copper–oxygen entities supported on the $\gamma$-alumina can be classified into several types:

*(a) Isolated $Cu^{2+}$ ions* can strongly interact with the support even to form the surface copper aluminate. They are separately isolated, so they have no spin–spin interaction. They can give a clear hyperfine structure in the EPR spectrum. They cannot be detected by XRD. *(b) Weak magnetic associates* consist of several or many $Cu^{2+}$ ions and these $Cu^{2+}$ ions have close contact with each other. Hence, they have poorly resolved hyperfine splitting in the EPR spectrum due to the dipolar coupling caused by the strong spin–spin interaction. They are not able to be detected by XRD. *(c) Small two- and three-dimensional clusters* have structures so loose that they have no specific and regular lattice arrangement. They cannot give rise to the hyperfine splitting in the EPR spectrum but give a EPR spectrum with weak signal intensity. They still cannot be detected by XRD due to their small particle size. *(d) Large three-dimensional clusters and bulk CuO phase* have characters and properties identical to those of pure CuO powder. Hence, they can be detected by XRD. Their spin coupling is too strong to create the EPR signal.

Combining the results of TPR and EPR, it can be found that the higher the copper loading is, the larger the $\gamma$-peak area of TPR and the weaker the signal intensity of EPR that will be obtained, while there is a maximum $\beta$-peak area of TPR appearing at 7.5 wt% Cu. These strongly suggest that the $\gamma$-peak copper oxide species belong to type *(d)* and the $\beta$-peak copper oxide species are composed of the types of *(a), (b)*, and *(c)*, because the signal intensity of EPR is proportional to the spin concentration of the isolated $Cu^{2+}$ ions (40).

Friedman *et al.* (20) reported that for CuO/$\gamma$-$Al_2O_3$ catalysts, saturation of the support surface occurs at a copper loading of approximately 4–5 wt% Cu per 100 $m^2$/g $\gamma$-$Al_2O_3$. Above this threshold loading, formation of crystalline CuO is observed. According to Friedman's saturation value, "monolayer" coverage of the support employed in this study (BET area = 169 $m^2$/g) should occur at a copper content of approximately 6.8–8.5 wt%. This value is compatible with the TPR results, which have displayed the maximum area of the $\beta$ peak occurring at 7.5 wt% Cu. Hence, the $\beta$ and $\gamma$ peak can be unambiguously attributed to the reduction of highly dispersed copper oxide species and bulk-like CuO, respectively.

Therefore, the increase in $\beta$-peak area following

reoxidation treatment can be interpreted as the increase of types *(a), (b)*, and *(c)* copper oxide species. This may exactly elucidate the reason why the dispersion of supported copper oxide catalyst can be increased after a reoxidation treatment (12, 28, 34). However, the total number of adsorption sites (for $Cu^{2+}$ ions) of the alumina support are finite; hence, the transformation between the $\beta$-peak and the $\gamma$-peak copper oxide species is limited. This coincides with the reoxidized TPR results that the absolute amount of reoxidized $\beta$-peak area of 10 wt% Cu is approximately identical to that of 12.5 wt% Cu, but there is an evident difference in their $\gamma$-peak areas.

### *4.2 Reduction Behavior of CuO/YSZ Catalyst*

In fact, reduction of metal oxide is also a heterogeneous catalytic reaction. The reactants are hydrogen and oxygen ions of metal oxide. Hence, the reduction of metal oxide also goes through the procedure of adsorption, surface reaction, and desorption. Based on the concept of the heterogeneous catalytic reaction, if there is a very active center appearing at the surface of metal oxide, the reduction should take place more easily and occur at lower temperature. Lo Jacono *et al.* (21) have pointed out that a good adsorbing site for the reduction of alumina-supported copper oxide should involve special configurations, such as coordinatively unsaturated surface $Al^{3+}$ ions, close to edges or other defects. Boon and co-workers (14) have confirmed that surface oxygen vacancies of copper oxide are the active sites for the TPR of the supported copper oxides.

From the viewpoint of catalytic oxidation reaction, if the reaction belongs to redox mechanism, the weaker the bond strength of oxygen ion is, the higher the catalytic activity that will be obtained. This aspect has been verified by many reactions, such as CO oxidation over vanadium oxide (13), high-temperature superconducting materials (15), and oxide catalysts (46); methanol oxidation over vanadium oxide (47); and hydrocarbon oxidation over metal oxides (19). These suggest that the weakly bonded oxygen ion can be removed more easily. For the same reason, if there is a weakly bonded oxygen ion existing on the surface of metal oxide, the reduction of this metal oxide should start from this position easily.

To sum up, the reduction of metal oxide needs some start points and the "trigger" of the reduction reaction may be a defect such as a surface oxygen vacancy or a weakly bonded surface oxygen ion. Hence, the $\alpha_1$-peak formation can be attributed to the hydrogen consumption of weakly bonded oxygen ions of copper oxide located on the surface oxygen vacancies of YSZ support. The $\alpha_2$-peak formation can be ascribed to the hydrogen consumption of the interfacial oxygen ions of copper oxide beside the surface oxygen vacancies of YSZ support. The reduction mechanisms are proposed and confirmed as follows.

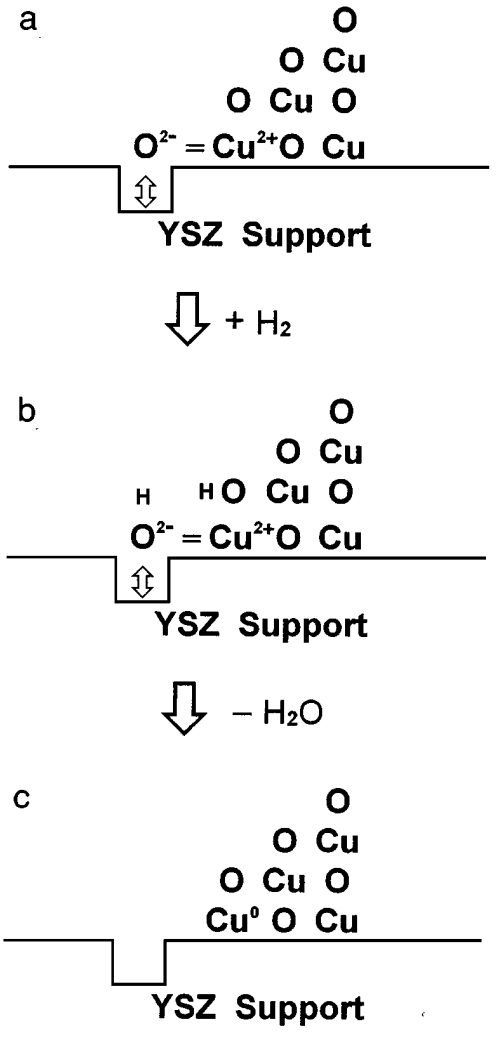


**FIG. 11.** Scheme of reduction mechanism I. (a), (b), and (c), see text; (⌐¬) surface oxygen vacancy of YSZ support.

*Reduction mechanism I.* When copper oxide is supported on the YSZ support, many copper oxide clusters should exist as illustrated in Fig. 11a. One interface-boundary terminal oxygen ion of the copper oxide cluster may locate on the surface oxygen vacancy of YSZ support. The surface defect structure of the YSZ proposed in Figs. 11–13 is according to the literature (29–32). Because YSZ is an outstanding oxygen ion conductor (29–32), the interface-boundary terminal oxygen ion of copper oxide may strongly interact with the surface oxygen vacancy and even incorporate into the vacancy after the catalyst has been calcined at 500°C. This strong affinity between the surface oxygen vacancy of YSZ and the interface-boundary terminal oxygen ion of copper oxide will cause this Cu=O bond to become weakened. We designate this oxygen ion as nested oxygen ion (NOI). As a result, once the hydrogen adsorbs on the catalyst, these NOIs will act as the trigger

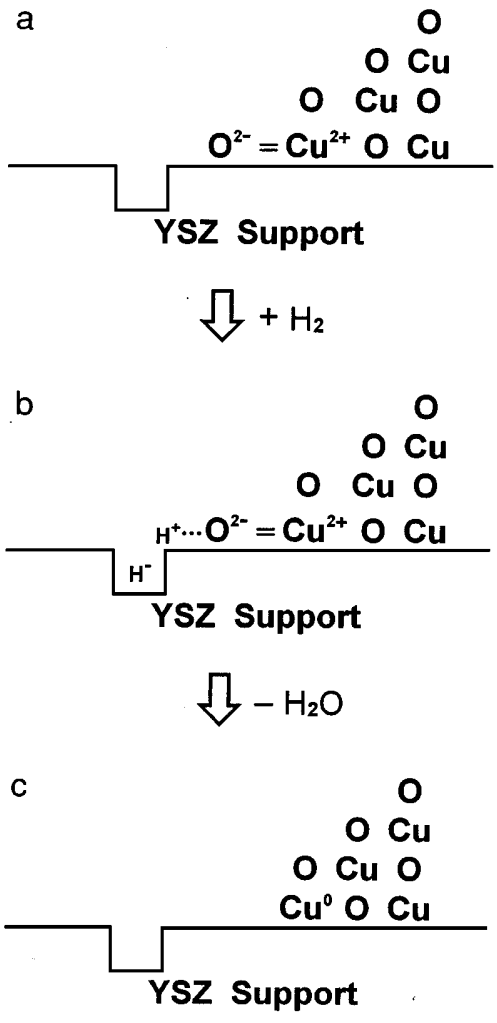


**FIG. 12.** Scheme of reduction mechanism II. (a), (b), and (c), see text; (⌐¬) surface oxygen vacancy of YSZ support.

for the reduction reaction of the CuO/YSZ catalyst. This reduction mechanism is shown in Fig. 11 and can also be manifested by

$$V_O^{\cdot\cdot} + O^{2-} = Cu^{2+} \rightarrow V_O^{\cdot\cdot} \cdots O^{2-} \cdots Cu^{2+} \qquad [1]$$

$$V_O^{\cdot\cdot} \cdots O^{2-} \cdots Cu^{2+} + H_2 \rightarrow V_O^{\cdot\cdot} + Cu + H_2O, \qquad [2]$$

where $V_O^{\cdot\cdot}$ is the oxygen vacancy of YSZ with a charge of +2. From Eq. [1], it can be seen that the bond strength between the NOI and $Cu^{2+}$ becomes weaker due to the interaction between the $V_O^{\cdot\cdot}$ and NOI, hence it can be withdrawn more easily by hydrogen.

*Reduction mechanism II.* If the interface-boundary terminal oxygen ion of copper oxide cluster locates beside the surface oxygen vacancy of YSZ, it can be illustrated as in Fig. 12a. For this case, the surface oxygen vacancies of YSZ can be regarded as the required defects for the reduction of copper oxide. In fact, the oxygen vacancies of YSZ have been verified to be good adsorbing sites for the adsorption of $SO_3$ and CO (16) and to be active sites for CO hydrogenation (16) and $C_4$ species formation (17). Many studies demonstrated that the adsorbed hydrogen prefer to incorporate to the oxygen vacancies of reducible supports such as $TiO_2$ (48, 49) and $CeO_2$ (50) during reduction. Moreover, because the oxygen vacancies of YSZ have positive charge (30, 32), it can functionally act as Lewis acid sites (17, 51). Therefore, when hydrogen passes through the CuO/YSZ catalyst, it may adsorb on the surface oxygen vacancies of YSZ and be thereupon activated by the oxygen vacancy to form a polarized species, $H^- \cdots H^+$, owing to the Lewis acid. This process is shown in Fig. 12b.

Lo Jacono *et al.* (21) have reported that during the reduction of the CuO/$\gamma$-$Al_2O_3$ catalyst, hydrogen prefers to adsorb on the surface defects of support and then the adsorbed hydrogen can be polarized by the defect to form the heterolytic dissociation $H^- \cdots H^+$. We think that once the adsorbed hydrogen is polarized by the surface oxygen vacancy, the basic group, $H^-$, prefers to insert into the Lewis acid site, whereas the acidic group, $H^+$, prefers to attack the $O^{2-}$ ion, which is a basic group in view of its bonding to copper.

Consequently, the interface-boundary terminal oxygen ions which are in the vicinity of the surface oxygen vacancies of YSZ will be easily withdrawn by the "corrosion" of acid. We designate these oxygen ions to be temptable oxygen ions (TOIs), because their removal is indirectly induced by the oxygen vacancies of YSZ. The reduction mechanism II is illustrated in Fig. 12 and can be represented alternatively by the following equations:

$$V_O^{\cdot\cdot} + H_2 \rightleftharpoons V_O^{\cdot\cdot} \cdots H^- \cdots H^+ \qquad [3]$$

$$V_O^{\cdot\cdot} \cdots H^- \cdots H^+ + O^{2-} = Cu^{2+} \rightarrow V_O^{\cdot\cdot} \cdots H^- \cdots H^+ \cdots O^{2-} \cdots Cu^{2+} \qquad [4]$$

$$V_O^{\cdot\cdot} \cdots H^- \cdots H^+ \cdots O^{2-} \cdots Cu^{2+} \rightarrow V_O^{\cdot\cdot} + Cu + H_2O. \qquad [5]$$

Here, one question, whether the $\alpha$-peak formation is due to the hydrogen consumption of interfacial oxygen ions of copper oxide clusters (i.e., NOIs and TOIs) instead of the isolated $Cu^{2+}$ ions, should be verified.

For the CuO/YSZ catalysts, their EPR signal intensities shown in Fig. 10 decrease with increasing copper content, but the maximum area of the $\alpha_1$ peak in the TPR patterns occurs at 0.4 wt% Cu instead of 0.2 wt% Cu. Therefore, the $\alpha_1$-peak generation cannot be attributed to the reduction of the isolated $Cu^{2+}$ ions, since the signal intensity of EPR is proportional to the spin concentration of isolated $Cu^{2+}$ ions (40). Consequently, the $\alpha_1$-peak formation is ascribed to the hydrogen uptake of NOIs, which are interface-boundary terminal oxygen ions of which the coordination environment belongs to the types of *(b)*, *(c)* or *(d)* as described in Section 4.1 and illustrated in Fig. 11a. In fact, as the copper

loading is increased to 1.5 wt% the hyperfine structure almost disappears completely, as shown in Fig. 10d, but the $\alpha$ peak still presents conspicuously in the TPR pattern. Hence, both NOIs and TOIs should be the oxygen ions of type *(b)*, *(c)*, or *(d)* copper oxide species. This also agrees with the results of chlorine addition that the $\alpha$-peak temperature can be markedly shifted by the added chlorine, which indicates that the $\alpha$-peak copper oxide species are not isolated copper ions (33).

### *4.3 Decipherment of Reduction Mechanisms for $\alpha_1$ and $\alpha_2$ Peaks*

After understanding the reduction mechanism, a subsequent question is to determine which mechanism is responsible for the $\alpha_1$- or $\alpha_2$-peak formation.

I. We undertake the consideration of the relationship between the dispersion and the particle size of the YSZ supported copper oxide. In Table 3, it is shown that the maximum value of the absolute amount of $\alpha_1$-peak area appears at 0.4 wt% Cu, but that of the $\alpha$-peak area (i.e., $\alpha_1+\alpha_2$) occurs at 0.6 wt% Cu. This suggests that when the copper loading exceeds 0.4 wt%, the amount of $\alpha_1$-peak copper oxide species will decrease with increasing copper loading. On the other hand, when the copper loading exceeds 0.4 wt%, the amount of $\alpha_2$-peak copper oxide species can still increase until the copper loading is larger than 0.6 wt% and then also decreases with further increase in copper loading. This implies that the amount of $\alpha_1$-peak copper oxide species is limited more easily by the copper loading than that of the $\alpha_2$-peak one. In other words, the $\alpha_1$-peak copper oxide species is more subject to its particle size.

Strohmeier and co-workers (22), using XPS and ISS (low energy ion scattering spectroscopy), demonstrated that below the saturated copper loading, i.e., 4–5 wt% Cu with respect to a surface area of 100 $m^2/g$ (20), the well-dispersed Cu species have a fairly constant particle size. The size and shape of the supported particles do not vary significantly for dispersed phase as also observed by Fung (52) and Kerkhof and Moulijn (53). Similar phenomena were also found by Hercules and co-workers over $Fe/Al_2O_3$ (54) and $V/Al_2O_3$ (55) catalysts. Taking account of the results of Table 3, this condition of so-called saturated copper loading seems to be also valid for the CuO/YSZ catalysts. This can be interpreted by the illustration of Fig. 13.

According to Friedman's rule (20) and the BET area of YSZ as shown in Table 1, the "saturated" copper loading should occur at 0.4 wt%. Hence, below this copper loading, the particle size should not vary significantly. This coincides with the EPR results, in which the EPR intensities of 0.2 and 0.4 wt% Cu/YSZ are approximately the same. After the copper loading goes higher than 0.4 wt%, there is a marked diminution of the EPR intensity. Based on these results, we propose a model shown in Fig. 13 to explain the results of Table 3.

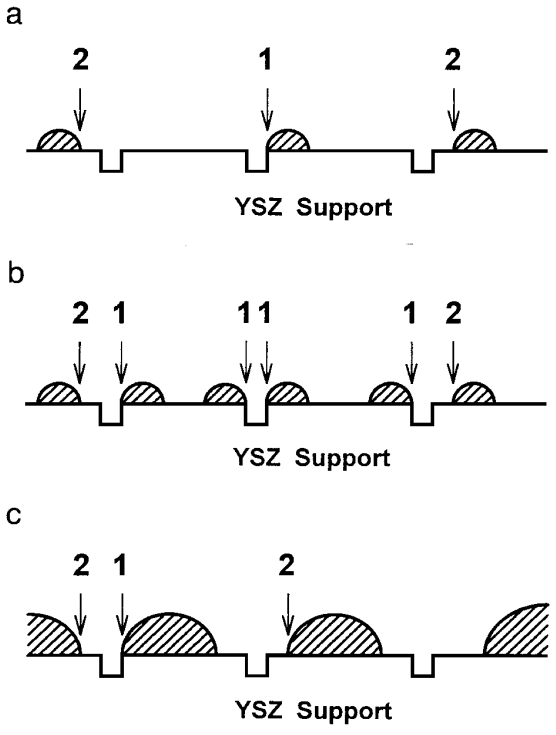


**FIG. 13.** A proposed model for the influence of copper loading on the particle size of copper oxide and on the number of NOIs and intrinsic TOIs. (a) The case for 0.2 wt% Cu, (b) the case for 0.4 wt% Cu, (c) the case for copper loading higher than 0.4 wt%, (1) position of NOI for reduction mechanism I; (2) position of intrinsic TOI for reduction mechanism II, (⌐⌙) surface oxygen vacancy of YSZ support, (▨) copper oxide particle.

The reduction mechanisms of the $\alpha_1$ and the $\alpha_2$ peaks can also be deduced from the results of Tables 3, 4, and 5.

Under a constant BET area of YSZ support, the number of the surface oxygen vacancies is finite. As the particle size of supported copper oxide is identical but small, as shown in Figs. 13a and 13b, the increase of crystallite number will lead to the extension of the interface-boundary line between the supported copper oxide and the YSZ. This will cause the concentration of NOI required for the reduction reaction of mechanism I to increase. When the copper loading is further

**TABLE 4**

**Ratios of $\alpha$ and $\alpha_1$ Peak Areas**

| Copper loading (wt%) | $\alpha/\alpha_1$[a] (mol $H_2$/mol $H_2$) |
|---|---|
| 0.2 | 5.96 |
| 0.4 | 2.02 |
| 0.6 | 2.69 |
| 0.8 | 3.05 |
| 1.0 | 3.11 |
| 1.5 | 3.45 |

[a] $\alpha$ Peak area $=\alpha_1$ peak area $+\alpha_2$ peak area.

**TABLE 5**

**The Estimative Concentration of Surface Oxygen Vacancy of YSZ**

| This work[a] (vacancy number/$m^2$) $\times 10^{17}$ | Ref. 16[b] (vacancy number/$m^2$) $\times 10^{17}$ | Ref. 56[c] (vacancy number/$m^2$) $\times 1$ |
|---|---|---|
| 1.84 (0.2 wt% Cu) | 4.98[d] | $10^{16}$–$10^{18}$ |
| 9.14 (0.4 wt% Cu) | 11.50[e] | |
| 7.79 (0.6 wt% Cu) | 11.90[f] | |
| 6.29 (0.8 wt% Cu) | 9.73[g] | |
| 6.07 (1.0 wt% Cu) | 25.90[h] | |
| 4.69 (1.5 wt% Cu) | | |

[a] evaluated from $\alpha_1$- peak areas of Table 3 for 8 mol% YSZ with BET area of 10 $m^2$/g.

[b] Evaluated by chemisorptive method of $SO_3$.

[c] A theoretically calculated value according to the unit cell of $ZrO_2$ lattice.

[d] For 7 mol% YSZ with BET area of 73.8 $m^2$/g.

[e] For 7 mol% YSZ with BET area of 29.5 $m^2$/g.

[f] For 9.1 mol% YSZ with BET area of 74.7 $m^2$/g.

[g] For 9.8 mol% YSZ with BET area of 96.4 $m^2$/g.

[h] For 9.8 mol% YSZ with BET area of 30.94 $m^2$/g.

increased and exceeds 0.4 wt%, these small crystallites begin to aggregate with each other, which has been confirmed by EPR. The aggregation of small copper oxide particles results in crystallite growth. Relatively, the number of NOI and TOI, especially NOI, is decreased due to the diminution of interface-boundary lines between the copper oxide clusters and the YSZ support. Furthermore, the larger the particle size of copper oxide, the higher the covering probability of the surface oxygen vacancies by the copper oxide clusters. This may explain the gradual decrease in both $\alpha_1$- and $\alpha_2$-peak areas when the copper loading is larger than 0.6 wt%.

Hence, as maximum area of $\alpha_1$ peak occurs at 0.4 wt%, it is certain that $\alpha_1$-peak species are NOIs, which belong to mechanism I. The $\alpha_2$ peak of the TPR is therefore attributed to the hydrogen consumption of TOIs, which belong to mechanism II.

II. From the viewpoint of stereo geometry, the hydrogen consumption of TOIs should be always larger than that of NOIs. This can be easily elucidated as follows.

(1) Considering an interfacial boundary of the copper oxide clusters with a large particle size, its boundary may be regarded as a straight line due to negligible curvature. Then one of the interface-boundary terminal oxygen ions of copper oxide clusters may meet the surface oxygen vacancy of YSZ to form a NOI,

$$\underset{\text{Cu}}{\overset{\text{O}}{\|}}\ \underset{\text{Cu}}{\overset{\text{O}}{\|}}\ \underset{\text{Cu}}{\overset{\text{O}}{\|}} + V_{\text{O}}^{\bullet\bullet} \rightarrow \underset{\text{Cu}}{\overset{\text{O}}{\|}}\ \underset{\text{Cu}}{\overset{[\text{O}]^{\text{N}}}{\|}}\ \underset{\text{Cu}}{\overset{\text{O}}{\|}}, \qquad [6]$$

where $[O]^N$ denotes NOI.

(2) NOI reacts with hydrogen to produce $H_2O$ and neighboring oxygen ions of copper oxide can simultaneously become TOIs due to the restored surface oxygen vacancy of YSZ,

$$\underset{\text{Cu}}{\overset{\text{O}}{\|}}\ \underset{\text{Cu}}{\overset{[\text{O}]^{\text{N}}}{\|}}\ \underset{\text{Cu}}{\overset{\text{O}}{\|}} + \text{H}_2 \rightarrow \underset{\text{Cu}}{\overset{\text{O}^{\text{T}}}{\|}}\ \underset{\text{Cu}}{\overset{V_{\text{O}}^{\bullet\bullet}}{\|}}\ \underset{\text{Cu}}{\overset{\text{O}^{\text{T}}}{\|}} + \text{H}_2\text{O}, \qquad [7]$$

where $O^T$ denotes TOI. These TOIs do not appear before reduction takes place for fresh catalysts, therefore we call these TOIs *extrinsic* TOIs in order to make discrimination with the case of mechanism II, which is an *intrinsic* TOI.

(3) Extrinsic TOIs react with hydrogen to produce $H_2O$:

$$\underset{\text{Cu}}{\overset{\text{O}^{\text{T}}}{\|}}\ \underset{\text{Cu}}{\overset{V_{\text{O}}^{\bullet\bullet}}{\|}}\ \underset{\text{Cu}}{\overset{\text{O}^{\text{T}}}{\|}} + 2\text{H}_2 \rightarrow 3\text{Cu} + V_{\text{O}}^{\bullet\bullet} + 2\text{H}_2\text{O}. \qquad [8]$$

Evidently, the concentration of TOI is always higher than that of NOI owing to the formation of *extrinsic* TOIs. Again, according to the integrated results of Table 3, it is certain that the reduction of $\alpha_1$-peak species belongs to mechanism I and the reduction of $\alpha_2$-peak species belongs to mechanism II. However, when the particle size of the supported copper oxide is small enough, the curvature of the interface-boundary line can no longer be neglected. A larger curvature will result in a smaller number of the *extrinsic* TOIs. In other words, the removal of one NOI may create only one or even no *extrinsic* TOI. This is the cases of 0.2 and 0.4 wt% Cu/YSZ catalysts as shown in Figs. 13a and 13b. Accordingly, most TOIs of 0.2 and 0.4 wt% Cu/YSZ catalysts should be intrinsic. The proof of the above inference will be given in Tables 4 and 5 and discussed below.

III. Considering the ratios of $\alpha/\alpha_1$ peak areas, Table 4 can give another telling clue and thereby makes the preceding discussion more convincing. It is conceivable that if the total number of the *intrinsic* and *extrinsic* TOIs is equal to that of NOI, the ratio of $\alpha/\alpha_1$ peak area should be two. On the other hand, if the number of NOIs is much lower than that of the sums of the *intrinsic* plus the *extrinsic* TOIs, then the ratio of $\alpha/\alpha_1$ peak area will be much greater than two. When the particle size of the supported copper oxide cluster becomes larger, the factor of stereo geometry should be taken into account. According to Eq. [7], the removal of one NOI may lead to the formation of two *extrinsic* TOIs; thus, if there is no *intrinsic* TOI, the ratio of $\alpha/\alpha_1$ peak area should be three.

Indeed, the results of Table 4 agree exactly with the above inference. The ratio of $\alpha/\alpha_1$ peak area of 0.2 wt% Cu/YSZ is much greater than two and that of 0.4 wt% Cu/YSZ is approximately equal to two. When the copper loading is further increased, the $\alpha/\alpha_1$ ratio approaches three until the copper loading reaches 1.0 wt%. The deviation from the ratio of three for higher copper loading means that when the particle size of supported copper oxide cluster is large

enough, the stereo geometric factor will become significant. It may generate one-dimensional, then two-dimensional, and finally three-dimensional *extrinsic* TOIs. Therefore, the $\alpha/\alpha_1$ ratio of 1.5 wt% Cu/YSZ can be much greater than three.

IV. If one documents the numerical value of the concentration of surface oxygen vacancy of YSZ support, the above-proposed three theories will be accordingly corroborated. One can imagine that if every one of the surface oxygen vacancies of YSZ support has been nested by the interface-boundary terminal oxygen ion of copper oxide to form the NOI after calcination, then the number of NOIs per BET area should equal that of the surface oxygen vacancies of YSZ. In practice, it seems impossible to make such an ideal surface state, because some surface oxygen vacancies may be covered by copper oxide particles at random or be vacant. Nevertheless, Table 5 shows that the estimative concentration of the surface oxygen vacancies of YSZ support which is evaluated from the $\alpha_1$-peak area coincides satisfactorily with that of references (16, 56), especially the magnitude of order. However, the total number of NOIs cannot represent all of the surface oxygen vacancies of the YSZ support. Hence, those values listed in the first column of Table 5 are more or less underestimated due to evaluating merely the $\alpha_1$-peak areas. The physical meaning of the numerical value variation for different copper loading, such as the minimum appearing in the case of 0.2 wt% Cu and the maximum occurring in the case of 0.4 wt% Cu and the progressive decrease from the case of 0.4 wt% Cu to that of 1.5 wt% Cu, can be easily elucidated by means of the illustration of Fig. 13. As shown in Fig. 13a, the copper loading is low and the particle number is small for the case of 0.2 wt% Cu, and thus most of the hydrogen uptake behavior of the interface-boundary terminal oxygen ions of copper oxide crystallites will comply with reduction mechanism II; hence, the NOIs are fewer then that seen with the TOIs and a higher ratio of $\alpha/\alpha_1$ results. When the copper loading exceeds 0.4 wt%, crystallite growth takes place and leads to the covering extent of the surface oxygen vacancies to be extended. Therefore, the estimative values in this work decrease with increasing copper loading. The maximal estimative value of the surface oxygen vacancy concentration is obtained from the case of 0.4 wt% Cu. This may exactly prove the foregoing discussion that the "optimal" distribution and particle size of the copper oxide crystallites should occur in the case of 0.4 wt% Cu. Hence, the surface oxygen vacancy concentration of the YSZ support evaluated from the case of 0.4 wt% Cu is very close to the real value.

### *4.4 Reduction Behavior of Reoxidized Cu/YSZ Catalyst*

The $\beta$ and the $\gamma$ peaks can be attributed to the reduction of the copper oxide species that possess different particle size and have no interaction and induction factor with the YSZ support and that have been denoted as case III copper oxide species in our previous report (12). Hence, their reduction and reoxidation behaviors are analogous to those of $CuO/\gamma$-$Al_2O_3$. In our previous study (12), we have proposed that the metal copper with a smaller particle size is easily split into several parts during reduction due to the surface oxygen vacancies of YSZ support. This can be supported by the reoxidized results of the $\beta$ peak in this work, which exhibit an easily redispersed behavior such that the latent $\beta$-peak with a higher temperature has become distinguishable with a lower temperature, as shown in Figs. 5 and 6.

After reoxidation treatment at 500°C, the TPR peak profiles and temperatures of the highly dispersed copper oxides or isolated copper ions (i.e., $\beta$-peak copper oxide species) are altered, but the $\alpha$-peak profiles and temperatures are almost not affected by the reoxidation treatment. Hence, once again, this indicates that the $\alpha$-peak formation is not due to the isolated copper ions.

### *4.5 Reduction Behavior of YSZ Support*

To the best of our knowledge, it seems that there is no TPR study of CuO/YSZ catalyst and YSZ support to date. In contrast to this, there are many TPR studies about zirconia (35–38). According to these reports (35–38), it is believed that zirconia can be partially reduced at high temperature, generally above 500°C, and that the reduction should occur only at the surface layer of zirconia.

Because YSZ has been widely used as a solid electrolyte for fuel cells (29, 30) with usual working temperatures of 800–1000°C, it is conceivable that YSZ should not be easily reduced by hydrogen. Nevertheless, many studies (57–59) have demonstrated that when YSZ is exposed either to reducing atmosphere or to electrical current at elevated temperature, it becomes colored due to reduction.

Before we explicate the reason for the $\delta$-peak formation of the YSZ support, it is necessary that some key points be emphasized:

(1) Yttria cannot be reduced in our current temperature range of reduction; therefore the reduction of yttria resulting in the formation of the $\delta$ peak can be ruled out. (2) Zirconia can be reduced when the temperature is higher than 550°C. However, its reduction rate is very low and thus a broadened and small TPR peak is obtained. On the other hand, the $\delta$ peak of YSZ support is very sharp as compared with that of $ZrO_2$, although its initial temperature is higher than that of $ZrO_2$. This means that once the reduction reaction starts, its rate is much higher than that of $ZrO_2$. (3) The profile of the $\delta$ peak can be modified by the supported copper. The higher the copper loading is, the lower the initial temperature of the $\delta$ peak that will be obtained. However, the hydrogen consumption of the $\delta$ peak is independent of the copper loading. (4) The structure of pure $ZrO_2$ is monoclinic, while YSZ has a cubic fluorite-type structure

and possesses many oxygen vacancies. Hence, the chemical property (reactivity) at their surface should be different.

Considering $CeO_2$, which is also an oxygen-ion conducting material and also possesses the cubic fluorite-type structure (30, 42–44), one will find that the TPR trace for the reduction of YSZ is very similar to that of $CeO_2$ except for bulk reduction (60–63). According to Yao and Yu Yao (60) and Johnson and Mooi (61), and TPR peak appearing at ca. 500°C for $CeO_2$ is attributed to the hydrogen consumption of surface capping oxygen anions which attach to surface $Ce^{4+}$ ions in an octahedral coordination.

Many studies (57–59) using EPR have demonstrated that when YSZ is heated in a hydrogen atmosphere at high enough temperature, paramagnetic signals which do not result from $Zr^{3+}$ ions and impurities are observed. These signals have been ascribed to the trapping of electrons in the charged variants of oxygen vacancies with or without an yttrium ion (57, 59) or to an electron trapped by a $Zr^{4+}$ ion perturbed by two oxygen vacancies placed at the opposite corners of the anions cube, that is, by a $Zr^{3+}$ ion in a trigonally distorted octahedral environment (58). Moreover, Azzoni and co-workers (64) further pointed out that the EPR signals of YSZ which result from lattice defects involving oxygen vacancies originate from the surface of YSZ.

To sum up the above discussion, it can be reasonably speculated that the $\delta$ peak is due to the hydrogen consumption of the surface capping oxygen ions of YSZ which locate beside the surface oxygen vacancies. The first step of the reduction mechanism is similar to that of the *intrinsic* TOIs proposed as shown in Fig. 12. The reduction steps can be depicted by means of the following equations.

(1) Hydrogen is activated by $V_O^{\bullet\bullet}$:

$$V_O^{\bullet\bullet} + H_2 \rightleftharpoons V_O^{\bullet\bullet}\cdots H^-\cdots H^+. \qquad [3]$$

(2) Surface capping oxygen ion of YSZ which locates beside the surface oxygen vacancy reacts with the polarized hydrogen,

$$V_O^{\bullet\bullet}\cdots H^-\cdots H^+ + O_c^{2-} \rightarrow V_O^{\bullet\bullet} + H_2O + 2e^-, \qquad [9]$$

where $O_c^{2-}$ is the surface capping oxygen ion.

(3) One of electrons released from the capping oxygen ion can be trapped by $Zr^{4+}$ to form $Zr^{3+}$ and the other is trapped by $V_O^{\bullet\bullet}$ to form $F^+$ center (57–59):

$$2e^- + Zr^{4+} \rightleftharpoons Zr^{3+} + e^- \qquad [10]$$

$$e^- + V_O^{\bullet\bullet} \rightleftharpoons F^+. \qquad [11]$$

(4) Both electrons released from the capping oxygen ion are simultaneously trapped by $V_O^{\bullet\bullet}$ to form F center (57, 59):

$$V_O^{\bullet\bullet} + 2e^- \rightleftharpoons F. \qquad [12]$$

Because the reduction of capping oxygen occurs only at the surface of YSZ, it is conceivable that it will be affected by the supported copper. In fact, it has been observed that the TPR peak temperature of capping oxygen ions of $CeO_2$ shifts downward after the precious metal is supported on it (60, 62, 63). This phenomenon has been attributed to hydrogen spillover from supported Group VIII metal to $CeO_2$ (62, 63, 65). However, it is well known that metal copper does almost not adsorb hydrogen, so it has been regarded as a poor catalyst for hydrogenation reactions (66). Therefore, the hydrogen spillover, of which the limiting step is hydrogen dissociation (65, 67), seems to be not a convincing explanation in our case.

Depending upon the result of Fig. 8, we propose a rational interpretation for the shift of the $\delta$-peak temperature after copper is supported on YSZ. It can be imagined that when the reduction temperature has exceeded 350°C, all of the supported copper oxides should have been reduced to metal coppers. Furthermore, the higher the temperature is, the higher the mobility of the surface oxygen vacancies will become. This will lead to a higher mobility and activity of the surface capping oxygen ions due to the oxygen-ionic transport via oxygen vacancies. Consequently, the activated surface capping oxygen ions of YSZ may thus be bonded to the metallic copper atoms to form shared oxygen ions, Zr–O–Cu.

Yao and Yu Yao (60) reported that once surface oxygen ions of $Al_2O_3$ could be shared with $CeO_2$, it could be easily removed by hydrogen. In addition, Deo and Wachs (47) pointed out that bridge-bonded vanadium oxide, Zr–O–V, is more reducible than that with a terminal bond (V=O). More recently, Brogan *et al.* (68) using Raman spectra confirmed that when Pt is supported on $CeO_2$, the surface capping oxygen anions can be easily removed at low reduction temperature owing to Pt–O–Ce linkage. In practice, these shared oxygen ions are similar to the NOIs; hence, they can be reduced more easily than unshared capping oxygen ions.

Therefore, the sharp profile of the $\delta$ peak can be attributed to the activation of surface capping oxygen ions due to the surface oxygen vacancies of YSZ. The relationship between the initial temperatures of the $\delta$ peaks and the copper loading can be ascribed to one capping oxygen ion being shared by not only one copper atom for the case of higher copper loading. In other words, the more copper sharers there are, the weaker the bond strength between the capping oxygen ion and zirconium ion is and the lower the reduction temperature that will be obtained. However, since the total surface oxygen vacancies and the capping oxygen ions are finite, the hydrogen consumption of the $\delta$ peak is independent of the copper loading.

Considering reaction [9], if one surface oxygen vacancy can cause only one surface capping oxygen ion to be reduced, then the surface oxygen vacancy concentration that is evaluated from the $\delta$-peak hydrogen consumption of

the YSZ support shown in Fig. 8 should be equal to that of Table 5. Without copper loading, the $\delta$-peak hydrogen consumption of YSZ support is $9.5–10 \times 10^{-6}$ mol for a sample weight of 0.2 g. Accordingly, the surface oxygen vacancy concentration is $28.3–29.8 \times 10^{17}$ (vacancy number/$m^2$). This value is very close to that of Refs. 16 and 56, as shown in Table 5. Compared with that of the first column of Table 5, the higher numerical value of surface oxygen vacancy concentration calculated from the $\delta$-peak hydrogen consumption can be reasonably ascribed to every surface oxygen vacancy being free because of no supported copper oxide.

## 5. CONCLUSIONS

1. When copper oxide is supported on $\gamma$-$Al_2O_3$, only two TPR peaks can be observed. One is attributed to the reduction of highly dispersed copper oxide species with a peak temperature of ca. 210°C; the other is ascribed to the reduction of bulky CuO with a peak temperature of ca. 245°C. According to the TPR and EPR results in this work and to the literature, it can be concluded that the highly dispersed copper oxide species should include the isolated copper ions, weak magnetic associates and small two- and three-dimensional clusters. The amounts of the highly dispersed copper oxide species can be increased and the amounts of the bulk-like CuO can be decreased by the reoxidation treatment due to the occurrence of redispersion.

2. When copper oxide is supported on YSZ, the interfacial terminal oxygen ions of copper oxide can be removed at a very low temperature to form third and fourth TPR peaks, i.e., $\alpha_1$ and $\alpha_2$ peaks, as well as $\beta$ and $\gamma$ peaks. $\alpha$-Peak formation has been attributed to the effect of surface oxygen vacancies of the YSZ support. These surface oxygen vacancies may either directly interact with the interfacial terminal oxygen ions of copper oxide or act as the adsorbing sites to polarize the adsorbed hydrogen due to their Lewis-acidic property.

3. The surface oxygen ions of the YSZ support can be removed by hydrogen and generate a small but sharp TPR peak at ca 657°C. These oxygen ions have been judged to be the surface capping oxygen ions which coordinate beside the surface oxygen vacancies of the YSZ support. These capping oxygen ions may be shared with supported copper atoms and thus its initial TPR peak temperature can be shifted downward due to the formation of bridging Cu–O–Zr bond.

## ACKNOWLEDGMENTS

This work was supported by the National Science Council of Republic of China under Contract NSC 83-0402-E-007-006. We are thankful to Miss Rou-Chyi Chen (National Science Council Regional Instrument Center, Hsinchu) for carrying out the EPR measurements.

## REFERENCES

1. Yu Yao, Y. F., *J. Catal.* **39**, 104 (1975).
2. Kummer, J. T., *Prog. Energy Combust. Sci.* **6**, 177 (1980).
3. Severino, F., Brito, J., Carias, O., and Laine, J., *J. Catal.* **102**, 172 (1986).
4. Dekker, N. J. J., Hoorn, A. J. J., Stegenga, S., Kapteijn, F., and Moulijn, J. A., *AIChE J.* **38**, 385 (1992).
5. Huang, T.-J., Yu, T.-C., and Chang, S.-H., *Appl. Catal.* **52**, 157 (1989).
6. Huang, T.-J., and Yu, T.-C., *Appl. Catal.* **71**, 275 (1991).
7. Stevenson, S. A., Dumesic, J. A., Baker, R. T. K., and Ruckenstein, E. (Eds.), "Metal–Support Interaction in Catalysis, Sintering and Redispersion." Van Nostrand-Reinhold, New York, 1987.
8. Haller, G. J., and Resasco, D. E., *Adv. Catal.* **36**, 173 (1989).
9. Metcalfe, I. S., and Sundaresan, S., *Chem. Eng. Sci.* **41**, 1109 (1986).
10. Metcalfe, I. S., and Sundaresan, S., *AIChE J.* **34**, 195 (1988).
11. Cho, B. K., *J. Catal.* **131**, 74 (1991).
12. Dow, W.-P., and Huang, T.-J., *J. Catal.* **147**, 322 (1994).
13. Roozeboom, F., Jos van Dillen, A., Geus, J. W., Gellings, P. J., *Ind. Eng. Chem. Prod. Res. Dev.* **20**, 304 (1981).
14. Boon, A. Q. M., van Looij, F., and Geus, J. W., *J. Mol. Catal.* **75**, 277 (1992).
15. Klissurski, D., and Rives, V., *Appl. Catal. A* **109**, 1 (1994).
16. Silver, R. G., Hou, C. J., and Ekerdt, J. G., *J. Catal.* **118**, 400 (1989).
17. Jackson, N. B., and Ekerdt, J. G., *J. Catal.* **126**, 31 (1990).
18. Jackson, N. B., and Ekerdt, J. G., *J. Catal.* **126**, 46 (1990).
19. Andersson, A., Hansen, S., and Sanati, M., *in* "Structure–Activity and Selectivity Relationships in Heterogeneous Catalysis" (R. K. Grasselli and A. W. Sleight, Eds.), p. 43, Elsevier, Amsterdam, 1991.
20. Friedman, R. M., Freeman, J. J., and Lytle, F. W., *J. Catal.* **55**, 10 (1978).
21. Lo Jacono, M., Cimino, A., and Inversi, M., *J. Catal.* **76**, 320 (1982).
22. Strohmeier, B. R., Leyden, D. E., Scott Field, R., Hercules, D. M., *J. Catal.* **94**, 514 (1985).
23. Dumas, J. M., Geron, C., Kribii, A., and Barbier, J., *Appl. Catal.* **47**, L9 (1989).
24. Tikhov, S. F., Paukshtis, E. A., Sadykov, V. A., Popovskii, V. V., Starostina, T. G., Kryukova, G. N., Kharlamov, G. V., Anufrienko, V. F., Poluboyarov, V. F., Razdobarov, V. A., Bulgakov, N. N., and Kalinkin, A. V., *Kinet. Catal.* **30**, 764 (1989).
25. Tikhov, S. F., Sadykov, V. A., Kryukova, G. N., Paukshtis, E. A., Popovskii, V. V., Starostina, T. G., Kharlamov, G. V., Anufrienko, V. F., Poluboyarov, V. F., Razdobarov, V. A., Bulgakov, N. N., and Kalinkin, A. V., *J. Catal.* **134**, 506 (1992).
26. Davydova, L. P., Fenelonov, V. B., Sadykov, V. A., Plyasova, L. M., and Anufrienko, V. F., *Kinet. Catal.* **34**, 85 (1993).
27. Lumbeck, H., and Voitländer, J., *J. Catal.* **13**, 117 (1969).
28. Deen, R., Scheltus, P. I. T., and de Vries, G., *J. Catal.* **41**, 218 (1976).
29. Etsell, T. H., and Flengas, S. N., *Chem. Rev.* **20**, 399 (1970).
30. Subbarao, E. C., Ed., "Solid Electrolytes and Their Applications." Plenum, New York, 1980.
31. Heuer, A. H., and Hobbs, L. W., (Eds.) "Science and Technology of Zirconia," Vol. 3. The American Ceramic Society, Ohio, 1981.
32. Subbarao, E. C., and Maiti, H. S., *Solid State Ionics* **11**, 317 (1984).
33. Dow, W.-P., and Huang, T.-J., *J. Catal.* **160**, 171 (1996).
34. Wolberg, A., and Roth, J. F., *J. Catal.* **15**, 250 (1969).
35. Shimokawabe, M., Asakawa, H., and Takezawa, N., *Appl. Catal.* **59**, 45 (1990).
36. Dall'Agnol, C., Gervasini, A., Morazzoni, F., Pinna, F., Strukul, G., and Zanderighi, L., *J. Catal.* **96**, 106 (1985).
37. Borer, A. L., Brönnimann, C., and Prins, R., *J. Catal.* **145**, 516 (1994).
38. Guglielminotti, E., Giamello, E., Pinna, F., Strukul, G., Martinengo, S., and Zanderighi, L., *J. Catal.* **146**, 422 (1994).
39. Berger, P. A., and Roth, J. F., *J. Phys. Chem.* **71**, 4307 (1967).
40. Blanco, J., Fayos, J., Gracía De La Banda, J. F., and Soria, J., *J. Catal.* **31**, 257 (1973).

41. Soria, J., Conesa, J. C., Martínez-Arias, A., and Coronado, J. M., *Solid State Ionics* **63–65**, 755 (1993).
42. Dell, R. M., and Hooper, A., *in* "Solid Electrolytes: General Principles, Characterization, Materials, Applications" (P. Hagenmuller and W. van Gool, Eds.), p. 291. Academic Press, New York, 1978.
43. Gerhardt-Anderson, R., and Nowick, A. S., *Solid State Ionics* **5**, 547 (1981).
44. Gerhardt-Anderson, R., and Nowick, A. S., *in* "Transport in Nonstoichiometric Compounds" (G. Simkovich and V. S. Stubican, Eds.), p. 111. Plenum, New York, 1985.
45. Abou Kaïs, A., Bennani, A., Aïssi, C. F., Wrobel, G., and Guelton, M., *J. Chem. Soc. Faraday Trans.* **88**, 1321 (1992).
46. Boreskov, G. K., *in* "Catalysis: Science and Technology" (J. R. Anderson, and M. Boudart, Eds.), Vol. 3, p. 108. Springer-Verlag, Berlin, (1982).
47. Deo, G., and Wachs, I. E., *J. Catal.* **146**, 323 (1994).
48. Conesa, J. C., Malet, P., Munuera, G., Sanz, J., and Soria, J., *J. Phys. Chem.* **88**, 2986 (1984).
49. Sanz, J., Rojo, J. M., Malet, P., Munuera, G., Blasco, M. T., Conesa, J. C., and Soria, J., *J. Phys. Chem.* **89**, 5427 (1985).
50. Munuera, G., Fernandez, A., and Gonzalez-Elipe, A. R., *in* "Catalysis and Automotive Pollution Control II" (A. Crucq, Ed.), p. 207. Elsevier, Amsterdam, 1991.
51. Méthivier, A., and Pijolat, M., *J. Catal.* **139**, 329 (1993).
52. Fung, S. C., *J. Catal.* **58**, 454 (1979).
53. Kerkhof, F. P. J. M., and Moulijn, J. A., *J. Phys. Chem.* **83**, 1612 (1979).
54. Hoffmann, D. P., Procter, A., Houalla, M., and Hercules, D. M., *J. Phys. Chem.* **95**, 5552 (1991).
55. Eberhardt, M. A., Houalla, M., and Hercules, D. M., *Surf. Interface Anal.* **20**, 766 (1993).
56. Fleming, W. J., *J. Electrochem. Soc.* **124**, 21 (1977).
57. Pai Verneker, V. R., Petelin, A. N., Crowne, F. J., and Nagle, D. C., *Phys. Rev. B* **40**, 8555 (1989).
58. Orera, V. M., Merino, R. I., Chen, Y., Cases, R., and Alonso, P. J., *Phys. Rev. B* **42**, 9782 (1990).
59. Azzoni, C. B., and Paleari, A., *Solid State Ionics* **44**, 267 (1991).
60. Yao, H. C., and Yu Yao, Y. F., *J. Catal.* **86**, 254 (1984).
61. Johnson, M. F. L., and Mooi, J., *J. Catal.* **103**, 502 (1987).
62. Trovaralli, A., Dolcetti, G., de Leitenburg, C., Kašpar, J., Finetti, P., and Santoni, A., *J. Chem. Soc. Faraday Trans.* **88**, 1311 (1992).
63. Yamada, T., Kayano, K., and Funabiki, M., *in* "New Aspects of Spillover Effect in Catalysts" (T. Inui, K. Fujimoto, T. Uchijima, and M. Masai, Eds.), p. 329. Elsevier, Amsterdam, 1993.
64. Azzoni, C. B., Paleari, A., Scardina, F., Krajewski, A., Ravaglioli, A., and Meschke, F., *J. Mater. Sci.* **28**, 3951 (1993).
65. El Fallah, J., Boujana, S., Dexpert, H., Kiennemann, A., Majerus, J., Touret, O., Villain, F., and Le Normand, F., *J. Phys. Chem.* **98**, 5522 (1994).
66. Satterfield, C. N., "Heterogeneous Catalysis in Industrial Practice," 2nd ed., pp. 1 and 175. McGraw–Hill, New York, 1991.
67. Teichner, S. J., *Appl. Catal.* **62**, 1 (1990).
68. Brogan, M. S., Dines, T. J., and Cairns, J. A., *J. Chem. Soc. Faraday Trans.* **90**, 1461 (1994).